The Thermal Expansion Of Ring Particles And The Secular Orbital Evolution Of Rings Around Planets And Asteroids

by

David Parry Rubincam

Planetary Geodynamics Laboratory

Code 698

Solar System Exploration Division

NASA Goddard Space Flight Center

Building 34, Room S280

Greenbelt, MD 20771

Correspondence:

David P. Rubincam

Planetary Geodynamics Laboratory

Code 698

Solar System Exploration Division

NASA Goddard Space Flight Center

Building 34, Room S280

Greenbelt, MD 20771

Voice: 301-614-6464

Fax: 301-614-6522

Email: David.P.Rubincam@nasa.gov

Abstract

The thermal expansion and contraction of ring particles orbiting a planet or asteroid can cause secular orbit evolution. This effect, called here the thermal expansion effect, depends on ring particles entering and exiting the shadow of the body they orbit. A particle cools off in the shadow and heats up again in the sunshine, suffering thermal contraction and expansion. The changing cross-section it presents to solar radiation pressure plus time lags due to thermal inertia lead to a net along-track force. The effect causes outward drift for rocky particles. For the equatorial orbits considered here, the thermal expansion effect is larger than Poynting-Robertson drag in the inner solar system for particles in the size range ~0.001 – 0.02 m. This leads to a net increase in the semimajor axis from the two opposing effects at rates ranging from ~0.1 R per million years for Mars to ~1 R per million years for Mercury, for distances ~2R from the body, where R is the body's radius. Asteroid 243 Ida has ~10 R per million years, while a hypothetical Near-Earth Asteroid (NEA) can have faster rates of ~0.5 R per thousand years, due chiefly to its small radius compared to the planets. The thermal expansion effect weakens greatly at Jupiter and is overwhelmed by Poynting-Robertson for icy particles orbiting Saturn. Meteoroids in eccentric orbits about the Sun also suffer the thermal expansion effect, but with only ~0.0003e^2 AU change in semimajor axis over a million years for a 2 m meteoroid orbiting between Mercury and Earth.

1. Introduction

Radiation forces (photon thrust) can cause the secular orbital evolution of small particles orbiting planets and asteroids. One of the best-known such forces is the Poynting-Robertson effect, which causes orbit decay for particles circling the Sun (Poynting, 1903; Robertson, 1937; Burns et. al, 1979). Similarly, it also causes orbit decay for ring particles orbiting a planet.

The Yarkovsky effects (diurnal, seasonal, and Yarkovsky-Schach) can also result in the secular orbital evolution of ring particles; for instance, those which compose Saturn's rings. A previous paper (Rubincam, 2006) dealt with how photon thrust from Yarkovsky thermal forces may affect the orbital evolution of Saturn's main rings (see also Vokrouhlicky et al., 2007). While it was found that Yarkovsky orbital evolution could be significant over the age of the solar system assuming no destruction of particles, the conclusion was tempered by the fact that all of the various Yarkovsky effects depend on the linkage between insolation (from the Sun or Saturn) and the orbit: particles must be in undisturbed principal axis rotation for the Yarkovsky mechanism to work optimally. Any disturbance in the linkage, such as from collisions, weakens Yarkovsky. Particles tumbling on timescales much shorter than the orbital period would tend to average out the effects to the point where Yarkovsky forces would become insignificant.

The diurnal and seasonal Yarkovsky effects also vanish at the opposite extreme of synchronous rotation; here there is too much linkage between orbit and insolation. Hence the Yarkovsky forces operate on a restricted set of rotational states.

The present paper examines yet another photon thrust effect, called here the thermal expansion effect. Like the Yarkovsky-Schach effect, it depends on particles entering and exiting the planet's shadow for its operation. And like the Yarkovsky-Schach effect, the thermal expansion effect tends to drive stony particles away from the planet, helping keep rings alive, thus working against forces like Poynting-Robertson and the seasonal Yarkovsky effect, which make ring particle orbits decay. Unlike the Yarkovsky effects, it is largely blind to spin state insofar as a particle's radial temperature distribution is concerned: particles can be in principal axis rotation, tumbling, or in synchronous rotation and still suffer the thermal expansion effect. Hence the effect is not

hampered by Yarkovsky's restrictive spin conditions. The effect does not work well in densely populated rings; neither does Yarkovsky. Therefore the thermal expansion effect will operate best in thinly populated rings, such as those around Jupiter and conjectured at Mars (e.g., Hamilton, 1996).

The basic idea behind the thermal expansion effect is qualitatively illustrated in Fig. 1. A spherical ring particle revolves in a circular orbit about a planet. Solar radiation pressure pushes on the particle, as denoted by the thick arrow. The direction of the force is away from the Sun, and the magnitude of the force is indicated by the size of the arrow. The force is proportional to the particle's cross-sectional area, which for a sphere is πR^2, where R is the particle's radius. Just before entering the shadow, the solar radiation pressure pushes on the particle in the direction of motion, which increases the semimajor axis. When the particle dives into the shadow the solar heating turns off, and the particle cools; thermal contraction causes the radius R to shrink. When the particle emerges from the shadow, solar radiation pressure acts against the motion so as to decrease the semimajor axis. However, the radius R upon emergence is smaller than when it went into the shadow, so that the solar radiation pressure is less. The Sun does warm the particle back up, increasing the radius, but this takes some time due to thermal inertia. As a result, the forces do not balance when averaging around the orbit, and the net effect is a positive along-track acceleration which increases the particle's orbital semimajor axis. The particle moves away from the planet.

The effect depends on both thermal expansion and contraction for its operation; it is called here the thermal expansion effect for short. It depends crucially on the particle's thermal inertia. If the particle heats up and cools down instantaneously and thus expands and contracts instantaneously, then the radii R at various points around the orbit is symmetrical with respect to the shadow, and the effect vanishes. At the other extreme, a particle with large thermal inertia will not heat up or cool down much, leading to little expansion or contraction and a small effect. Hence somewhere between the extremes the effect works best.

The quantitative treatment of the thermal expansion effect follows. It is based on the formalisms of Rubincam (1987, 1998, 2006). The ring particles are in circular orbits about the planet. The particles are assumed to be made of rock in the case of Jupiter and

planets and asteroids sunward of Jupiter, while for Saturn the particles are composed of water ice. In all cases the particles are taken to be opaque spheres with homogeneous properties. The particles are assumed to be far enough apart from each other so that the shadowing or illumination of one particle by another can be ignored; in other words, the rings are sparsely populated.

The present paper concentrates on rocky equatorial rings around the terrestrial planets (though none have been observed) and Jupiter (which definitely has rings), and the water ice rings of Saturn. It also looks at two asteroids: 243 Ida, and a hypothetical NEA (Near-Earth Asteroid). Uranus, Neptune, and Pluto are ignored, due to the weakness of the effect thanks to their great distance from the Sun. The ring particle orbits are assumed to remain circular; changes in orbital eccentricity e are not considered. Readers uninterested in the mathematics can skip to section 6.

2. Insolation on ring particles

The ring geometry is shown in Fig. 2. The Sun is in the x-z plane. A particle orbits in the planet's equatorial plane in a circular orbit at a distance a from the planet's center. Its angular position ϕ in the equatorial plane is measured from the x-axis. The insolation incident on the particle can be written as a Fourier series

$$F_{Sun} = F_E \left(\frac{a_E}{a_{Plan}} \right)^2 \left[b_0 + \sum_{j=1}^{\infty} b_j \cos j\phi \right] \tag{1}$$

where F_E = 1361 W m^{-2} is the solar flux at the Earth (Kopp and Lean, 2011), a_E = 1 AU is the semimajor axis of the Earth's orbit, and a_{Plan} is the semimajor axis of the planet's orbit about the Sun. For Mars, for instance, a_{Plan} = 1.52 AU. Also, $\phi = nt$, where t is time and

$$n = \left(\frac{GM_{Plan}}{a^3} \right)^{1/2} \tag{2}$$

is the mean motion of the particle, with M_{Plan} being the planet's mass and G being the universal constant of gravitation.

The coefficients b_j express the fact that sunlight turns off when the particle enters the planet's shadow and turns back on when it exits the shadow. It will be assumed here that the Sun is a point source, and that there is no refraction of sunlight by the planet's atmosphere into the dark region behind it. In other words, the transition from full sunlight to complete darkness is instantaneous; thus (1) expresses a "boxcar" function. In this case

$$b_0 = 1 - \Lambda, \tag{3}$$

and

$$b_j = 2\sin\left[j(1-\Lambda)\pi\right]/\pi, \tag{4}$$

where Λ is the fraction of the orbit which is shadowed (e.g., Rubincam, 2006), so that Λ ranges from 0 (orbits outside the shadow) to 1/2 (orbits hugging the planet).

3. Ring particle temperatures

The variable insolation will cause the temperature T of the particle to fluctuate. The temperature distribution inside the particle can be found from the heat diffusion equation

$$K\nabla^2 T = \rho C_p \frac{\partial T}{\partial t}$$

(e.g., Chapman, 1967), where K is thermal conductivity, ρ is density, and C_p is specific heat; K, ρ, and C_p are taken to be constant throughout the particle. Temperature T can be written $T = T_0 + \Delta T$, where T_0 is a constant in space and time. Only the radial temperature distribution inside the particle will be considered here, so that $\Delta T = \Delta T(r)$, where r is the distance from the center of the particle. The above equation then reduces to

$$\frac{K}{r^2}\frac{\partial\left(r^2\frac{\partial T}{\partial r}\right)}{\partial r} = \rho C_p \frac{\partial T}{\partial t} \quad . \tag{5}$$

Switching to complex form, the time-dependence of F_{Sun} can be written in terms of $\exp(i\nu t)$, where $i = (-1)^{1/2}$ and ν is the frequency of the jth term in (1), so that $\nu = jn$. It is well-known that for each term in the insolation (1) there will be a corresponding term in the temperature of the form ΔT_j = constant $\times\, j_0(kr)\exp(i\nu t)$, where

$$j_0(kr) = \frac{\sin kr}{kr} \tag{6}$$

is the spherical Bessel function of order zero, and

$$k = \left(\frac{-i\nu\rho C_p}{K}\right)^{1/2} \quad .$$

If the particle radiates like a grey body, then the thermal emission will vary like T^4. The constant in ΔT can be found from linearizing the power balance at the surface $r = R_0$, where R_0 is the radius of the particle, using the approximation $T^4 \approx {T_0}^4 + 4{T_0}^3\,\Delta T$, so that

$$K\left.\frac{\partial(\Delta T)}{\partial t}\right|_{r=R_0} + 4\varepsilon_{IR}\sigma {T_0}^3 \Delta T = (1 - A_V)F_{Sun}/4 \quad .$$

Here A_V is the particle's albedo in the visible, ε_{IR} is the infrared emissivity, and σ is the Stefan-Boltzmann constant. The factor of 4 on the right side comes from the solar flux being incident on $\pi {R_0}^2$ and being averaged over the particle's surface area of $4\pi {R_0}^2$. Writing $\Delta T = \Sigma_j\, \Delta T_j(r)$, by the above equation

$$\Delta T_j(r) = \frac{(1-A_V)b_j F_E R_0}{4K}\left(\frac{a_E}{a_{Plan}}\right)^2\left(\frac{zj_0(kr)}{z\cos z + c_0 \sin z}\right)e^{i\nu t} \tag{7}$$

with $z = kR_0 = x(1 - i)$ and

$$x = R_0\left(\frac{\nu\rho C_p}{2K}\right)^{1/2} \quad , \tag{8}$$

with c_0 being

$$c_0 = \frac{4\varepsilon_{IR}\sigma T_0^{\,3} R_0}{K} - 1 \quad . \tag{9}$$

At the surface of the particle a typical temperature term by (7) is

$$\Delta T_j(R_0) = \frac{(1-A_V)b_j F_E R_0}{4K}\left(\frac{a_E}{a_{Plan}}\right)^2\sqrt{\frac{B_1^2 + B_2^2}{B_3^2}}e^{i(\nu t - \delta_j)} \quad , \tag{10}$$

where

$$\frac{zj_0(z)}{z\cos z + c_0 \sin z} = \frac{B_1 - iB_2}{B_3} \quad ,$$

with

$$B_1 = x\,(\sin 2x + \sinh 2x) + c_0\,(\cosh 2x - \cos 2x), \tag{11}$$

$$B_2 = x\,(\sinh 2x - \sin 2x), \tag{12}$$

$$B_3 = 2x^2\,(\cosh 2x + \cos 2x) + 2c_0 x\,(\sinh 2x + \sin 2x) + c_0{}^2\,(\cosh 2x - \cos 2x), \tag{13}$$

and

$$\tan \delta_j = \frac{B_2}{B_1} \quad . \tag{14}$$

4. Ring particle thermal expansion and contraction

Because of temperature changes inside the particle, the molecules at r will be displaced radially a distance $u(r)$ due to thermal expansion and contraction. Elasticity theory says $u(r)$ is given by the expression

$$u(r) = \frac{\alpha_V (1+\sigma_P)}{9(1-\sigma_P)} \left[\frac{1}{r^2} \int_0^r r^2 \Delta T(r)\, dr + \frac{2r(1-2\sigma_P)}{R_0^3 (1+\sigma_P)} \int_0^{R_0} r^2 \Delta T(r)\, dr \right] \quad , \tag{15}$$

where α_V is the volume expansion coefficient and σ_P is Poisson's ratio (Landau and Lifshitz, 1970, p. 22). The radius of the particle will be given by $R = R_0 + \Delta R$. At the surface (15) becomes

$$\Delta R = u(R_0) = \frac{\alpha_V}{3R_0^2} \int_0^{R_0} r^2 \Delta T(r) dr \tag{16}$$

and Poisson's ratio drops out. This equation is obviously correct when ΔT is just a constant; in this case $\Delta R = (\alpha_V/3)\Delta T R_0$, where $\alpha_V/3$ is the linear expansion coefficient.

The equation (7) for $\Delta T(r)$ contains the spherical Bessel function (6). The Bessel function is sin kr/kr, where k is complex and

$\sin kr = \sin (qr - iqr) = \cosh qr \sin qr - i \sinh qr \cos qr$.

Here $q = x/R_0$. Using the above expressions in (16) results in the integrals

$$\int r\cosh qr\sin qr\,dr = \frac{r}{2q}\left(\sinh qr\sin qr - \cosh qr\cos qr\right) + \frac{1}{2q^2}\sinh qr\cos qr$$

and

$$\int r\sinh qr\cos qr\,dr = \frac{r}{2q}\left(\cosh qr\cos qr + \sinh qr\sin qr\right) - \frac{1}{2q^2}\cosh qr\sin qr\ ,$$

ultimately giving

$$\Delta R = \frac{\alpha_V(1-A_V)R_0^2F_E}{4K}\left(\frac{a_E}{a_{Plan}}\right)^2\sum_{j=1}^{\infty}h_j\cos\left(j\phi-\zeta_j\right)$$

$$= \frac{\alpha_V(1-A_V)R_0^2F_E}{4K}\left(\frac{a_E}{a_{Plan}}\right)^2\sum_{j=1}^{\infty}h_j(\cos\,j\phi\cos\zeta_j+\sin\,j\phi\sin\zeta_j)\quad . \tag{17}$$

In (17)

$$h_j = b_j\sqrt{\frac{D_1^2+D_2^2}{D_3^2}}\quad , \tag{18}$$

where

$$D_1 = [(1 + c_0)\,x\,(\sinh 2x - \sin 2x)]/4x^2, \tag{19}$$

$$D_2 = \{x\,(\sinh 2x + \sin 2x) - 2x^2\,(\cosh 2x + \cos 2x) + c_0\,[\cosh 2x - \cos 2x - x\,(\sinh 2x + \sin 2x)]\}/4x^2, \tag{20}$$

and

$$D_3 = B_3/2\ . \tag{21}$$

Also,

$$\tan \zeta_j = \frac{D_2}{D_1} \quad . \tag{22}$$

5. Ring particle along-track acceleration

With the equation for ΔR in hand, the acceleration due to the thermal expansion and contraction can now be found. The acceleration of the particle due to solar radiation pressure is

$$\ddot{\mathbf{r}} = -\frac{\pi R^2 C_R F_{Sun}}{cM} \hat{\mathbf{r}}_\mathbf{S} \tag{23}$$

where c is the speed of light,

$$M = 4\pi\rho R^3/3 \tag{24}$$

is the mass of the particle, C_R is the radiation pressure coefficient, and F_{Sun} is given by (1). For a diffusely reflecting sphere $C_R \approx 1.2$ (e.g., Smith et al., 1991); this is the value adopted here.

Assuming $\Delta R << R_0$, so that $R^2 \approx {R_0}^2 + 2R_0\,\Delta R$, the acceleration due to the change in radius is (dropping the subscript on R_0)

$$\ddot{\mathbf{r}}_\mathbf{EX} = -\frac{2\pi R \Delta R C_R F_{Sun}}{cM} \hat{\mathbf{r}}_\mathbf{S} \quad , \tag{25}$$

where

$$\hat{\mathbf{r}}_\mathbf{S} = \cos\varepsilon_V \hat{\mathbf{x}} + \sin\varepsilon_V \hat{\mathbf{z}}$$

is the unit vector in the direction from the planet's center to the Sun, with ε_V being the solar elevation angle; $\varepsilon_V = 0$ when the Sun is in the planet's equatorial plane.

It remains to find how thermal expansion affects the orbital evolution. For a particle in a circular orbit, the change in the semimajor axis a with time t is

$$\frac{da}{dt} = \frac{2S_{EX}}{n} \tag{26}$$

(e.g., Blanco and McCuskey, 1961), where

$$S_{EX} = \hat{\mathbf{t}} \cdot \ddot{\mathbf{r}}_{\mathbf{EX}}$$

is the along-track acceleration due to the expansion effect, with

$$\hat{\mathbf{t}} = -\sin\phi\,\hat{\mathbf{x}} + \cos\phi\,\hat{\mathbf{y}}$$

being the unit vector in the direction of motion. By the above and (25)

$$S_{EX} = \ddot{\mathbf{r}}_{\mathbf{EX}} \cdot \hat{\mathbf{t}} = \frac{2\pi R C_R}{cM} \cos\varepsilon_V \Delta R (F_{Sun} \sin\phi) \ , \tag{27}$$

where

$$F_{Sun}\sin\phi = F_E \left(\frac{a_E}{a}\right)^2 \left[\left(b_0 - \frac{b_2}{2}\right)\sin\phi + \left(\frac{b_1}{2} - \frac{b_3}{2}\right)\sin 2\phi \right.$$

$$\left. + \left(\frac{b_2}{2} - \frac{b_4}{2}\right)\sin 3\phi + ...\right] \ ,$$

so that

$$F_{Sun}\sin\phi = \frac{F_E}{2}\left(\frac{a_E}{a_{Plan}}\right)^2\left\{\sum_{m=1}^{\infty}\left[\left(1+\delta_{1m}\right)b_{m-1}-b_{m+1}\right]\sin m\phi\right\} \quad , \tag{28}$$

with δ_{mj} being the Kronecker delta: $\delta_{mj} = +1$ when $m = j$ and is zero otherwise. Plugging (17) and (28) into (27) yields terms with factors of the form $\sin j\phi \sin m\phi$, among others. Using

$$\sin j\phi \sin m\phi = [\cos(j-m)\phi - \cos(j+m)\phi]/2$$

and retaining only the first term on the right side for which $j = m$ yields the secular terms in S_{EX}, resulting in

$$\bar{S}_{EX} = \frac{3\alpha_V(1-A_V)C_R F_E^2\cos\varepsilon_V}{32K\rho c}\left(\frac{a_E}{a_{Plan}}\right)^4\sum_{j=1}^{\infty}\left[(1+\delta_{1j})b_{j-1}-b_{j+1}\right]h_j\sin\zeta_j \quad . \tag{29}$$

The above expression gives the along-track acceleration averaged over one orbital revolution about the planet. It is interesting that the semimajor axis a does not appear in the coefficient multiplying the sum. It is implicit in the variables in the summation.

The planet's year must be averaged over next, because the tilt of the planet's axis causes ε_V to constantly change. The b_j in (29) are functions of ε_V and a; how much shadow is cast on the ring system depends on the solar elevation angle and the distance of the rings from the planet. The shadow cast on the equatorial plane is an ellipse, with a semimajor axis $R_{Plant}/\sin\varepsilon_V$ and semiminor axis R_{Plan}, where R_{Plan} is the planet's radius. A particle passes through the shadow when the circle of radius a and the shadow ellipse intersect. The intersection points can be found from the equations for the circle

$$\frac{x^2}{a^2}+\frac{y^2}{a^2}=1$$

and the ellipse

$$\frac{x^2}{\left(\dfrac{R_{Plan}}{\sin \varepsilon_V}\right)^2} + \frac{y^2}{R_{Sat}^2} = 1,$$

yielding

$$\Lambda = \frac{2\,\mathrm{Arc}\sin\left[\dfrac{\left(R_{Plan}^2 - a^2 \sin^2 \varepsilon_V\right)^{1/2}}{a\cos\varepsilon_V}\right]}{2\pi}, \tag{30}$$

which is to be used in (3) and (4). The solar elevation ε_V varies with time according to sin ε_V = sin ε sin ($2\pi t/P_{Plan}$), where for example $\varepsilon = 25°$ is the obliquity of Mars' equator, and P_{Plan} = 1.6 yr is the length of the Martian year in Earth years. Due to the complexity of (30), at this point the analytical development is forsaken for a numerical one in order to average (29) over the planet's year.

The ring particle temperature T_0 will be found from

$$4\varepsilon_{IR}\sigma T_0^4 = F_E\left(\frac{a_E}{a_{Plan}}\right)^2\left[b_0\left(1-A_V\right) + \frac{A_{Plan}(1-A_V)}{4}\left(\frac{R_{Plan}}{a}\right)^2 + \frac{\xi(1-A_{Plan})(1-A_{IR})}{4}\left(\frac{R_{Plan}}{a}\right)^2\right] \tag{31}$$

The first term in the brackets is the average amount of sunlight shining directly on the particle. The second term gives the heating of the particle from visible light reflected off of the planet, where A_{Plan} the planet's albedo in the visible (Conrath et al., 1989); here it is assumed that the body reflects uniformly off its surface. The third term in the brackets gives the heating of the particle from infrared radiation coming up from the planet; A_{IR} is the particle's albedo in the infrared. The parameter ξ accounts for whether the planet emits more energy than it absorbs from the Sun. In the case of the terrestrial planets, it is assumed that ξ = 1, since the geothermal flux is much smaller that solar insolation.

However, ξ = 1.67 for Jupiter and 1.78 for Saturn. In other words, Saturn and Jupiter each have a significant source of internal energy (Conrath et al., 1989). It is assumed in this term that the planet's infrared radiation is emitted uniformly.

It should be noted that T_0 computed via (31) is not the same as the average temperature T_{avg} obtained by measuring temperatures over space and time and taking the numerical average; instead $T_{avg} < T_0$ (Rubincam, 2004). The temperature dependence of K and C_p is computed using T_0 in the following sections. Using T_{avg} would be a better choice, especially in the case of Saturn, where the ice particle temperatures may be close to 73 K, which is the temperature where the thermal expansion effect changes sign for polycrystalline ice (see section 9). However, the difference between T_0 and T_{avg} is ignored here, due to the complications of finding T_{avg}.

6. Ring particle orbital evolution

The rings are assumed to be made of rock for the asteroids and planets, except for Saturn; there the rings are taken to be composed of water ice. For rock, each ring particle has a density of ρ = 3000 kg m^{-3} and has a constant visible albedo A_V = 0.05, infrared albedo A_{IR} = 0.1, and infrared emissivity ε_{IR} = 0.9. The volume coefficient of thermal expansion for rock is simply assumed to be a constant

$$\alpha_V = 15 \times 10^{-6}$$

regardless of T_0, while the thermal conductivity K and specific heat C_p are respectively assumed to depend on temperature the way basalt does:

$$K = 3.0 - 0.002\ T_0 \text{ W m}^{-1} \text{ K}^{-1}$$

and

$$C_p = 500 + 0.833\ T_0 \text{ J kg}^{-1} \text{ K}^{-1}$$

(Roy et al., 1981, p. 434-435). Parameters for seven planets and two asteroids are given in Table 1. Further, in (29), the summation is cut off at $j = 19$.

The Poynting-Robertson along-track acceleration S_{PR} is also estimated here. It is taken to be

$$S_{PR} = -\frac{3F_E[\xi(1-A_{Plan})+A_{Plan}]}{16c^2\rho R}\left(\frac{a_E}{a_{Plan}}\right)^2\left(\frac{R_{Plan}}{a}\right)^2 v \qquad (32)$$

where $v = na$ is the speed of the particle in its circular orbit (Burns et al., 1979). The equation for S_{PR} assumes the planet's visible and infrared radiation is isotropic around the planet. Direct solar radiation pressure, the Yarkovsky effects, atmospheric and plasma drag, electric charging, magnetic fields, the solar wind, gravitational perturbations from other bodies (such as satellites), and the lumpy gravitation field of the body itself are all ignored. Only the Poynting-Robertson effect is considered here in addition to the thermal expansion effect.

7. Rocky rings around Jupiter and the inner planets

Figures 3-9 show *da/dt* for rocky particles in terms of planetary radii per 10^6 years as a function of distance from the orbited body, where *da/dt* is the sum of the thermal expansion effect (29) plus the Poynting-Robertson effect (32):

$$\frac{da}{dt} = 2(S_{EX} + S_{PR})/n \quad . \qquad (33)$$

The figures show *da/dt* for four particle sizes: $R = 0.001$ m, 0.005 m, 0.01 m, and 0.02 m. Sizes below 0.001 m are not shown because they give unstable results, apparently due to the number of terms used in the Fourier expansion of the shadow and to the approximate equations used here. Fewer Fourier terms increases the instability, as does being far from the orbited planet where the particles spend less time in shadow.

For the particle sizes and distances from the planet (1.1 - 7.0 R_{Plan}) considered here, da/dt is positive for the inner planets; the thermal expansion effect is stronger than the Poynting-Robertson effect and the ring particles move outward. But for Jupiter and beyond the Poynting-Robertson effect can be stronger close to the planet for some particle sizes; in that case, $da/dt < 0$ and the rings move inward.

Mercury (Fig. 3) shows the fastest ring particle orbital revolution in terms radii per million years compared to the other inner planets. The mean motion n in (33) does not show much variation for the inner planets, being roughly 0.001 $N^{-3/2}$ s^{-1} for all of them, where $N = a/R_{Plan}$, so that the mean motion does not account for much of the differences in ring evolution in (33). Rather, Mercury is fast because its radius in small compared to Venus, Earth, and Mars, which appears to make it speedier in terms of the chosen units; and because it is closest to the Sun. It will be noted from (29) that the thermal expansion effect goes like square of the solar flux, i.e., $F_E^2(a_E/a_{Plan})^4$, for the following reason: not only does the thermal expansion of a particle depend on the solar flux, but also the force on it also depends on solar radiation pressure (Fig. 1); hence the square. On the other hand, Poynting-Robertson depends on the flux coming up from the planet, which depends linearly on the light the planet receives from the Sun. Hence Poynting-Robertson varies only like the solar flux $F_E(a_E/a_{Plan})^2$ itself. For Mercury, the Poynting-Robertson effect, though also strong near the Sun, seldom accounts for more than ~15% of the thermal expansion effect for the sizes considered.

Venus and Earth (Fig.s 4 - 5) have nearly the same radius and mass. Venus's orbital evolution is ~4 times the Earth's, mainly owing to Venus being closer to the Sun. At the Earth, the Poynting-Robertson effect is ~20% of the thermal expansion for 0.001 m particles close to the Earth, and turns out to be larger than the thermal expansion effect at distances > 9 R_{Earth} (not shown in Fig. 5, which cuts off at 7 R_{Earth}).

Mars (Fig. 6) and Earth have nearly identical curves in terms of planetary radii per million years because while Mars is further from the Sun, which weakens the effect, Mars has only half the radius of the Earth, which appears to hasten its orbital evolution in the chosen units. The vertical dotted lines in Fig. 6 show the positions of Phobos and Deimos, which are possible sources of dust. At Jupiter (Fig. 7) the Sun is so weak that ring evolution is very slow, and the Poynting-Robertson effect with its high velocities

dominates close to the planet. The shaded areas in Fig. 7 show the approximate locations of the halo ring, the main rings, and the Amalthea gossamer ring. The Thebe gossamer ring is not shown.

8. Rocky rings of Ida and an NEA

The results for a hypothetical Near-Earth Asteroid (NEA) are shown in Fig. 8. The NEA is assumed to be a sphere with radius R_{NEA} = 1000 m, density ρ = 2000 kg m^{-3}, in the same orbit as the Earth (a_{NEA} = 1 AU), and with the same obliquity (23.5°). In this figure *da/dt* is measured in asteroid radii per thousand years, rather than per million years. The reason for the apparently quickened pace in Fig. 8 is the NEA's small radius.

Figure 9 shows the rates of orbital evolution for rocky rings around asteroid 243 Ida. Ida is assumed to be a sphere here with a radius $R_{Ida} = 1.57 \times 10^4$ m, but in reality the asteroid is highly elongated. Measured in terms of Ida radii per million years, *da/dt* appears fast due to the asteroid's small size.

9. Icy rings of Saturn

Water ice can be polycrystalline, single crystals, or amorphous. Only the polycrystalline phase is considered here because the observed thermal inertia of the rings is so low. The ice is assumed to be "fluffy", with a density ρ = 500 kg m^{-3} rather than the 918 kg m^{-3} of a solid piece of ice. For polycrystalline ice K = 0.0001 W m^{-1} K^{-1} (Spilker et al., 2003; Ferrari et al., 2005), and $C_p = 715.0 + 8.2733\ (T_0 - 80.0)$ J kg^{-1} K^{-1} (Giauque and Stout, 1936).

As for visible albedos used in (31), the observed albedos vary from ring to ring: for the C ring, $0.17 < A_V < 0.48$, while for the B ring $0.41 < A_V < 0.73$ and for the A ring $0.31 < A_V < 0.63$ (Porco et al., 2005). Here the visible albedos A_V are simply taken to be 0.35 in the C ring (1.1-1.5 R_{Sat}) , 0.8 in the B ring (1.5-2.0 R_{Sat}), and 0.5 in the A ring and beyond (2.0-7.0 R_{Sat}), where R_{Sat} is the radius of Saturn. The least-known parameters in (31) are the infrared albedo A_{IR} and infrared emissivity ε_{IR}; these are simply set to A_{IR} = 0.15 and ε_{IR} = 0.85 for all three rings.

The volume coefficient of thermal expansion α_V can be found from Hobbs (1974, p. 347), who plots the observed linear thermal expansion of polycrystalline water ice as a function of temperature T (circles in Fig. 10). After converting Hobbs' linear expansion to volume expansion by multiplying by a factor of 3, α_V follows the approximate equation

$$\alpha_V \approx 3\ [0.0017\ (T_0 - 10.0)^2 - 6.75] \times 10^{-6}\ K^{-1} \qquad (34)$$

for polycrystalline water ice. This equation is the solid line plotted in Fig. 10 and is used as the expression for α_V. The line reproduces the polycrystalline curve quite well in the temperature range 30 - 130 K. The parameters were chosen so that (34) crosses $\alpha_V = 0$ exactly at T_0 = 73 K, as does the observed polycrystalline curve. Hence (34) is a reasonable approximation for α_V for the temperatures encountered at Saturn.

When $\alpha_V > 0$ the particles are driven away from Saturn, as shown in Fig. 1. For temperatures below 73 K, Fig. 10 indicates that $\alpha_V < 0$ for polycrystalline ice, so that particles with low average temperatures would actually be driven toward Saturn and the rings would collapse. For sparsely populated rings the temperatures are near 73 K and the rings may expand or collapse from the thermal expansion effect, depending upon the exact temperature.

Figure 11 shows the results for Saturn. In this figure $T_0 > 73$ K everywhere. The approximate positions of the C, B, and A rings are denoted by the grey areas. The Poynting-Robertson effect dominates the thermal expansion effect for Saturn, and these rings would collapse from the combination of the two effects for the size range indicated.

11. Meteoroids orbiting the Sun

Meteoroids in eccentric orbits about the Sun will also suffer from the thermal expansion effect. The meteoroid's radius will increase from solar heating as it approaches the Sun, but will not reach its maximum radius until after perihelion passage because of thermal inertia (Fig. 12). Far from the Sun the meteoroid cools and contracts, lessening solar radiation pressure. As in shadow passage, radiation pressure acts asymmetrically on

the orbit, increasing both semimajor axis a and the eccentricity e. The acceleration (25) will be of order

$$e^2 H \frac{C_R(1-A_V)\alpha_V}{\rho c K} F_E^2 \left(\frac{a_e}{a}\right)^4$$

by (17), where

$$H = \sqrt{\frac{D_1^2 + D_2^2}{D_3^2}} \sin\zeta \quad .$$

H reaches a maximum of ~0.0066 at radius ~2 m for a rocky meteoroid in an orbit which takes it between Mercury and the Earth (details omitted). This leads to a secular rate of change in the semimajor axis of $da/dt = \sim 0.0003\ e^2$ (AU/10^6 y), where e is the orbital eccentricity. The eccentricity e itself will also change secularly, but the changes in both a and e are tiny.

Dmitrievskii (1981) considers the effect thermal expansion has on the motion of a meteoroid's perihelion, but assumes no thermal lags. Without the lags there are no secular effects on a and e.

11. Discussion

In computing orbital evolution, all rings are assumed to be sparsely populated: the ring particles are taken to be far enough apart so that mutual shadowing can be ignored. All ring particles are also assumed to stay in circular orbits in the equatorial plane of the body they orbit. Staying in such orbits for long periods of time would probably require the rings to be densely populated enough for mutual collisions to kill any developing orbital eccentricities or inclinations. Hence there is something of a contradiction: on the one hand the rings assumed to be sparsely populated, but on the other hand populated densely enough for collisions.

More serious is the issue of particle lifetimes. The other forces mentioned in section 6 which might influence the lifetimes are all ignored here. Hamilton and Burns (1992), for instance, find that solar radiation pressure is very efficient in increasing orbital eccentricities for small particles orbiting asteroids until the particles crash into the surface. Thermal stresses have been neglected. These stresses could lead to cracking and comminution of particles as they constantly plunge in and out of the planet's shadow and their temperatures plummet and skyrocket. Any hysteresis in the expansion-contraction cycle is also ignored. Impacts, perhaps the most important destroyer of ring particles, have been neglected as well (Durisen, 1984; Durisen et al., 1996).

The results indicate that the thermal expansion effect, though weak, outweighs the Poynting-Robertson effect for a limited range of sizes. As particles become smaller they become nearly isothermal and the thermal lags are tiny, so that the thermal expansion effect becomes negligible, while the rate of Poynting-Robertson drag increases. Thus for the smaller-sized particles, probably not much smaller than the lower limit of R = 0.001 m investigated here, the Poynting-Robertson effect dominates.

How does the sum of the thermal expansion effect plus Poynting-Robertson effect (TE + PR) compare with the sum of the seasonal Yarkovksy effect plus Yarkovsky-Schach effect (SY + YS)? While no detailed comparison is given here, for the terrestrial planets they are roughly equal at $a = 2\ R_{Plan}$ when R = ~0.02 m. At smaller sizes TE + PR dominates, while at larger sizes SY + YS dominates. (SY and YS for these planets were computed using the equations from Rubincam (2006); the seasonal effect was averaged over all spin axis positions.) Hence the thermal expansion dominates in the narrow niche ~0.001 m to ~0.02 m between Poynting-Robertson and Yarkovsky.

Where might the thermal expansion effect be most significant, if at all? Ring particles have to exist for the thermal expansion effect to work on them. No rings are expected for Mercury and Venus because they lack an orbital source, and no rings have been observed. O'Keefe (1980) speculated that the Earth once had tektite rings; Hancock and Povenmire (2010) conjecture remnants may still survive. But the prospects for rings around the three innermost planets appear poor.

NEAs might produce debris from Yarkovsky-O'Keefe-Radzieevski-Paddack (YORP) spin-up (Paddack, 1969; Rubincam, 2000), from YORP fissioning (e.g.,

Jacobson and Scheeres, 2011), from tidal encounters with planets (e.g., Richardson et al., 1998), or from impacts. Moreover, the thermal expansion timescale is fast compared to the asteroid's radius (Fig. 8), which should help orbital debris stay in orbit. However, one suspects the timescales of solar radiation pressure (Hamilton and Burns, 1992) and the asteroid's lumpy gravitational field are much faster still, overwhelming the thermal expansion effect for NEAs as well as for main-belt asteroids. Further, the Poynting-Robertson effect from an NEA is so weak that a fully relativistic treatment may produce solar Poynting-Robertson terms (Rubincam, submitted manuscript, 2013).

Jupiter has rocky rings (e.g., Burns et al., 1984, 1999), but the planet is far from the Sun and its environment is not as benign for small particles as that of the inner planets. But it is intriguing that Poynting-Robertson drag dominates thermal expansion for the smaller particle sizes at the inner edge of Jupiter's halo ring (Fig. 7). Inside the inner edge particles fall on Jupiter, while outside they are pushed away by the thermal expansion effect. Saturn's icy rings have plenty of particles, but the planet is almost twice as far from the Sun as Jupiter, where the effect is already weak, so it is doubtful it plays much of a role at Saturn.

Probably the best candidate is Mars, though so far no rings have been observed there (Showalter et al., 2006). Its moons Phobos and Deimos would supply the dust, and Mars is close enough to the Sun for the thermal expansion effect to be relatively strong (Fig. 6), helping keep rings alive.

What about the thermal expansion effect operating on meteoroids orbiting the Sun? The effect requires an initial orbital eccentricity e to work. Due its weakness and the fact that it depends on e^2, the effect is unlikely to have much application to meteoroids.

Acknowledgments

I thank Susan Fricke for excellent programming support. The support of the AES and SALMON proposals is gratefully acknowledged.

References

Blanco, V. M., McCuskey, S. W., 1961. Basic Physics of the Solar System. Addison-Wesley, Reading, Mass.

Burns, J. A., Lamy, P. L., Soter, S. 1979. Radiation forces on small particles in the solar system. Icarus 40, 1-48.

Burns, J. A., Showalter, M. R., Morfill, G. E., 1984. The ethereal rings of Jupiter and Saturn. In Greenberg, R., Brahic, A. (Eds.), Planetary rings. Univ. Arizona Press, Tucson, pp. 200-272.

Burns, J. A., Showalter, M. R., Hamilton, D. P., Nicholson, P. D., de Pater, I., Ockert-Bell, M. E., Thomas, P. C., 1999. The formation of Jupiter's faint rings. Science 284, 1146-1150. doi: 10.1126/science.284.5417.1146.

Chapman, A. J. 1967. Heat Transfer, 2nd ed. Macmillan, New York.

Conrath, B. J., Hanel, R. A., Samuelson R. E., 1989. Thermal structure and heat balance of the outer planets, in: Atreya, S. K., Pollack, J. B., and Matthews, M. S. (Eds.), Origin and Evolution of Planetary and Satellite Atmospheres, Univ. Arizona Press, Tucson, pp. 513-538.

Dmitrievskii, A. A., 1981. Motion of the perihelion of a meteor orbit due to thermally induced expansion of the meteor. Solar System Research 14, 183-186.

Durisen, R. H. 1984. Transport effects due to particle erosion mechanisms, in: Greenberg, R., Brahic, A. (Ed.s), Planetary Rings, Univ. Arizona Press, Tucson, pp. 416-446.

Durisen, R. H., Bode, P. W., Dyck, S. G., Cuzzi, J. N., Dull, J. D., White, J. C., 1996. Ballistic transport in planetary ring mechanisms due to particle erosion mechanisms. III. Torques and mass loading by meteoroid impacts. Icarus 124, 220-236.

Ferrari, C., Galdemard, P., Lagage, P.O., Pantin, E., Quoirin, C., 2005. Imaging Saturn's rings with CAMIRAS: thermal inertia of B and C rings. Astron. Astrophys. 441, 379-389.

Giauque, W. F., Stout, J. W., 1936. The entropy of water and the third law of thermodynamics. The heat capacity of ice from 15 to 273°K. J. Amer. Chem. Soc. 58, 1144-1150.

Hamilton, D. P., 1996. The asymmetric time-variable rings of Mars. Icarus 119, 153-172. doi: 10.1006/icar.1996.008.

Hamilton, D. P., Burns, J. A., 1992. Orbital stability zones about asteroids. III. The destabilizing effects of eccentric orbits and of solar radiation. Icarus 96, 43-64.

Hancock, L.,O., Povenmire, H., 2010. Earth: a ringed planet? Amer. Geophys. U., Fall Meeting 2010, San Francisco. Abstract no. P23B-1635.

Hobbs, P. V., 1974. Ice Physics. Clarenden, Oxford.

Jacobson, S. A., Scheeres, D. J., 2011. Dynamics of rotationally fissioned asteroids: Source of observed small asteroid systems. Icarus 214, 161-178. doi: 10.1016/j.icarus.2011.04.009.

Kopp. G., Lean, J. L., 2011. A new, lower value of total solar irradiance: Evidence and climate significance. Geophys. Res. Lett. 38, L01706. doi: 10.1029/2010GL045777.

Landau, L. D., Lifshitz, E. M., 1970. Theory of Elasticity, 2nd ed., Pergamon, New York.

O'Keefe, J. A., 1980. The terminal Eocene event: formation of a ring system around the Earth? Nature 285, 309-311.

Paddack, S. J., 1969. Rotational bursting of small celestial bodies: effects of radiation pressure. J. Geophys. Res. 74, 4379-4381.

Porco, C., Baker, E., Barbara, J., Beurle, K., Brahic, A., Burns, J. A., Charnoz, S., Cooper, N., Dawson, D. D., Del Genio, A. D., Denk, T., Dones, L., Dyudina, U., Evans, M. W., Giese, B., Grazier, K., Helfenstein, P., Ingersoll, A. P., Jacobson, R. A., Johnson, T. V., McEwen, A., Murray, C. D., Neukum, G., Owen, W. M., Perry, J., Roatsch, T., Spitale, J., Squyres, S., Thomas, P., Tiscareno, M., Turtle, E., Vasavada, A. R., Ververka, J., Wagner, R., West, R. 2005. Cassini imaging science: initial results on Saturn's rings and satellies. Science 307, 1226-1236.

Poynting, J. H., 1903. Radiation in the solar system; its effect on science on temperature and its pressure on small bodies. Mon. Not. R. Astron. Soc. 72 (appendix), 265-266.

Richardson, D. C., Bottke, W. F., Love, S. G., 1998. Tidal distortion and disruption of Earth-crossing asteroids. Icarus 134, 47-76. doi: 10.1006/icar.1998.5954.

Robertson, H. P., 1937. Dynamical effects of radiation in the solar system. Mon. Not. R. Astron. Soc. 97, 423-437.

Roy, R. F., Beck, A. E., Touloukian, Y. S., 1981. Thermophysical properties of rocks, in:. Touloukian, Y. S., Judd, W.R., Roy, R. F. (Ed.s), Physical properties of rocks and minerals, McGraw-Hill, New York, pp. 409-502.

Rubincam, D. P., 1987. LAGEOS orbit decay due to infrared radiation from Earth. J. Geophys. Res. 92, 1287-1294.

Rubincam, D. P., 1998. Yarkovsky thermal drag on small asteroids and Mars-Earth delivery. J. Geophys. Res. 103, 1725-1732.

Rubincam, D. P., 2000. Radiative spin-up and spin-down of small asteroids. Icarus 148, 2-11.

Rubincam, D. P., 2004. Black body temperature, orbital elements, the Milankovitch precession index, and the Seversmith psychroterms. Theor. Appl. Climatol. 79, 111-131. doi: 10.1007/s00704-004-0056-5.

Rubincam, D. P. 2006. Saturn's rings, the Yarkovsky effects, and the ring of fire. Icarus 184, 532-542.

Showalter, M. R., Hamilton, D. P., Nicholson, P. D., 2006. A deep search for Martian dust rings and inner moons using the Hubble Space Telescope. Planet. Space Sci. 54, 844-854. doi: 10.1016/j.pss.2006.05.009.

Smith, D. E., Kolenkiewicz, R., Dunn, P. J., Klosko, S. M., Robbins, J. W., Torrence, M. H., Williamson, R. G., Pavlis, E. C., Douglas, N. B., Fricke, S. K., 1991. LAGEOS Geodetic Analysis—SL7.1. NASA Tech. Mem. 104549.

Spilker, L., Ferrari, C., Cuzzi, J. N., Showalter, M., Pearl, J., Wallis, B., 2003. Saturn's rings in the thermal infrared. Planet. Space Sci. 51, 929-935.

Vokrouhlicky, D., Nesvorny, D., Dones, L., Bottke, W. F., 2007. Thermal forces on planetary ring particles. Astron. Astrophys. 471, 717-730. doi: 10.1051/0004-6361:20067029.

Table 1. Parameters for seven planets and two asteroids.

Object	a_{Plan}[a] (AU)	M_{Plan}[b] (10^{24} kg)	R_{Plan}[c] (10^6 m)	ε[d] (deg)	A_{Plan}[e]	ξ[f]
Mercury	0.39	0.330	2.440	1.0	0.07	1.0
Venus	0.72	4.869	6.052	2.6	0.90	1.0
Earth	1.00	5.974	6.391	23.5	0.31	1.0
NEA	1.00	8.378×10^{-12}	0.001	23.5	0.05	1.0
Mars	1.52	0.642	3.389	25.0	0.25	1.0
Ida	2.86	4.2×10^{-8}	0.016	1.0	0.08	1.0
Jupiter	5.20	1898.6	71.492	3.13	0.52	1.67
Saturn	9.58	568.8	60.330	26.73	0.34	1.78

[a] Semimajor axis of the object's orbit.

[b] Mass.

[c] Radius.

[d] Obliquity.

[e] Visible albedo.

[f] Ratio of energy emitted to that received from the Sun.

Figures

Fig. 1. Schematic of the thermal expansion effect. A ring particle orbits around a body; the view is looking down on the particle's orbital plane. Sunlight (wavy lines) causes radiation pressure on the particle (thick arrows). The size of the arrows indicates the magnitude of the force. Sunlight heats the particle, making it expand, increasing radiation pressure. Shadow passage (grey region) causes particle contraction, decreasing radiation pressure. The forces do not balance around the orbit because of thermal inertia, causing the orbit to expand secularly.

Fig. 2. Schematic of a particle's orbit. A particle P is in a circular, equatorial orbit around a body. Its distance from the center of the body is a. The Sun lies in the x-z plane, with elevation angle ε_V.

Fig. 3. Mercury ring particle rates of orbital evolution da/dt as a function of distance for the combined thermal expansion effect and the Poynting-Robertson effect, for stony particles with radii of 0.001 m, 0.005 m, 0.010 m, and 0.02 m. The particles are assumed to be in circular orbits. The abscissa is distance from the center of the planet, measured Mercury radii R_{Merc}. The ordinate is given in terms of R_{Merc} per 10^6 years. The curves may differ slightly from their actual values due to the "quantum" nature of PowerPoint™ graphs.

Fig. 4. Same as Fig. 3, but for Venus.

Fig. 5. Same as Fig. 3, but for Earth.

Fig. 6. Same as Fig. 3, but for Mars.

Fig. 7. Same as Fig. 3, but for Jupiter.

Fig. 8. Graph similar to Fig. 3, but for a hypothetical spherical NEA with radius 1000 m and density 2000 kg m^{-3} and in Earth's orbit with Earth's obliquity. The ordinate is in radii per 10^3 years, instead of per 10^6 years as in the other figures.

Fig. 9. Same as Fig. 3, but for asteroid 243 Ida, assuming Ida is a sphere.

Fig. 10. The measured volume coefficient expansion for polycrystalline water ice as a function of temperature (circles) and the curve assumed here. The coefficient is negative for temperatures below 73 K, so that the thermal expansion effect would cause orbital decay rather than expansion for temperatures below this value.

Fig. 11. Same as Fig. 3, but for ice particles orbiting around Saturn.

Fig. 12 Schematic of the thermal expansion effect for a meteoroid in an eccentric orbit about the Sun. The size of the arrows indicates the magnitude of solar radiation pressure on the meteoroid. As it approaches the Sun, sunlight (wavy arrows) heats up the meteoroid more and more, making it expand, increasing its cross-section and thus the force. The meteoroid achieves maximum size after perihelion passage, thanks to thermal inertia. Far from the Sun the weakened sunlight causes the meteoroid to contract, decreasing radiation pressure. The forces do not balance around the orbit, causing the orbit to expand secularly. The thermal expansion effect will also secularly change the orbital eccentricity.

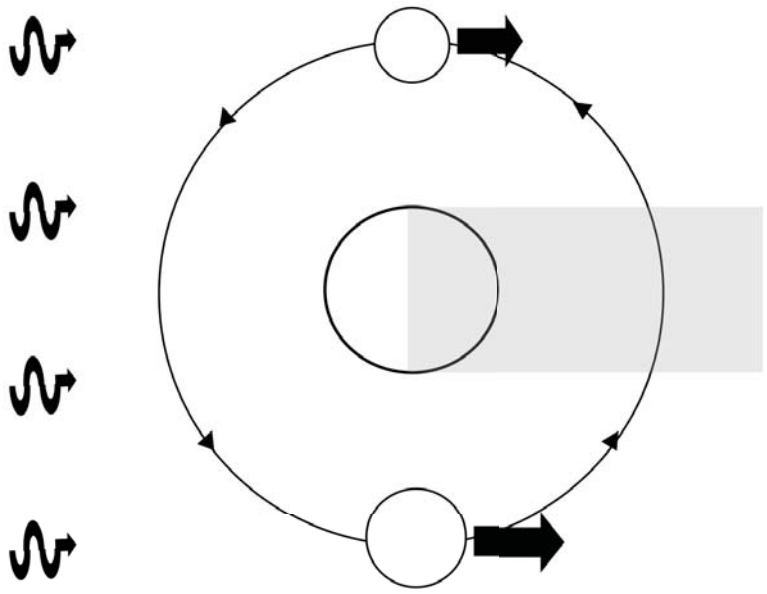

Fig. 1. Schematic of the thermal expansion effect. A ring particle orbits around a body; the view is looking down on the particle's orbital plane. Sunlight (wavy lines) causes radiation pressure on the particle (thick arrows). The size of the arrows indicates the magnitude of the force. Sunlight heats the particle, making it expand, increasing radiation pressure. Shadow passage (grey region) causes particle contraction, decreasing radiation pressure. The forces do not balance around the orbit because of thermal inertia, causing the orbit to expand secularly.

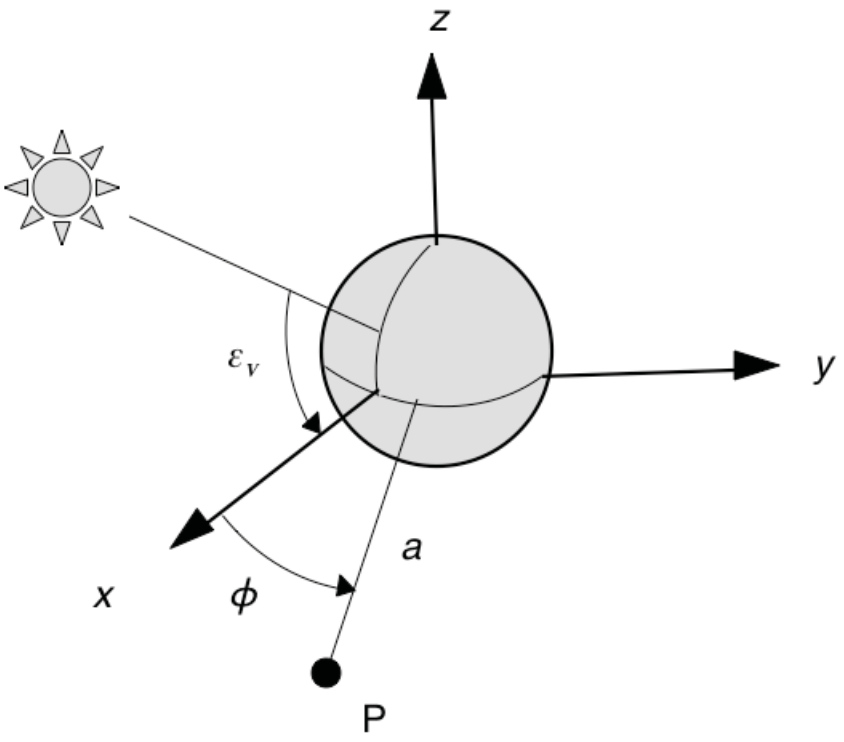

Fig. 2. Schematic of a particle's orbit. A particle P is in a circular, equatorial orbit around a body. Its distance from the center of the body is *a*. The Sun lies in the *x*-*z* plane, with elevation angle ε_V.

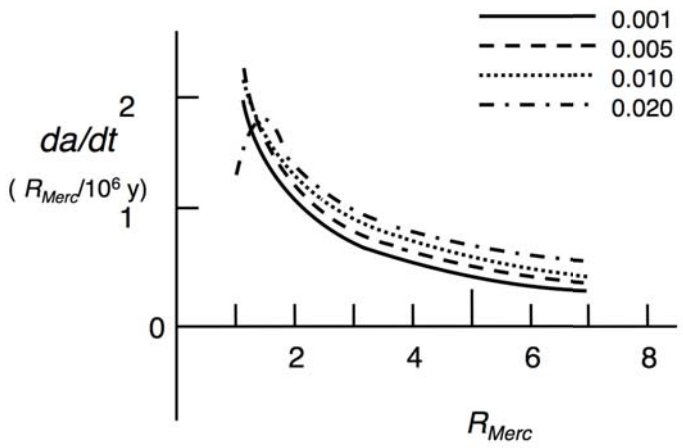

Fig. 3. Mercury ring particle rates of orbital evolution *da/dt* as a function of distance for the combined thermal expansion effect and the Poynting-Robertson effect, for stoney particles with radii of 0.001 m, 0.005 m, 0.010 m, and 0.02 m. The particles are assumed to be in circular orbits. The abscissa is distance from the center of the planet, measured Mercury radii R_{Merc}. The ordinate is given in terms of R_{Merc} per 10^6 years. The curves may differ slightly from their actual values due to the "quantum" nature of PowerPoint™ graphs.

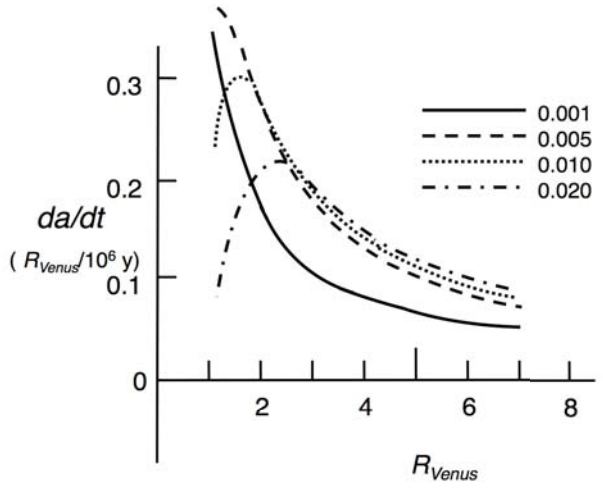

Fig. 4. Same as Fig. 3, but for Venus.

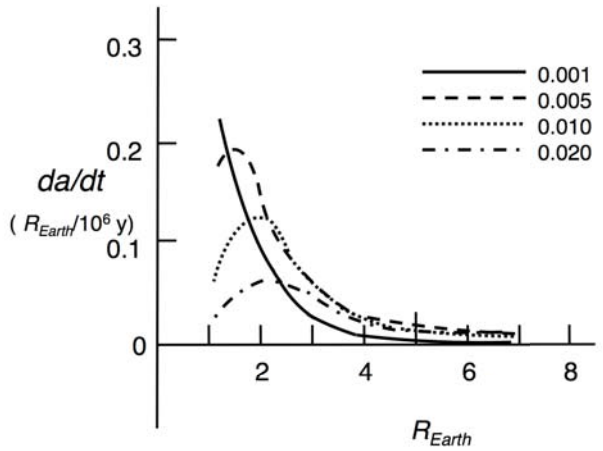

Fig. 5. Same as Fig. 3, but for Earth.

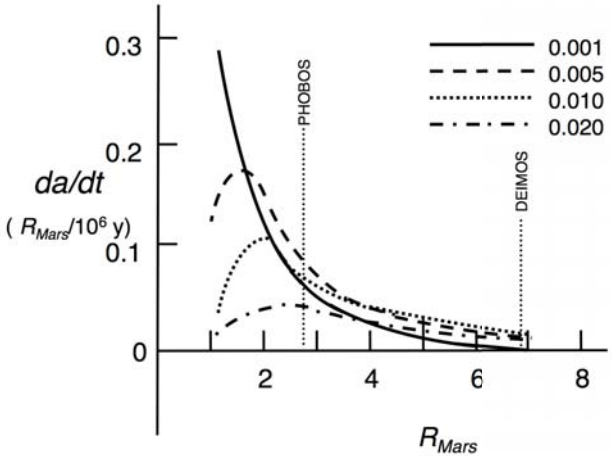

Fig. 6. Same as Fig. 3, but for Mars.

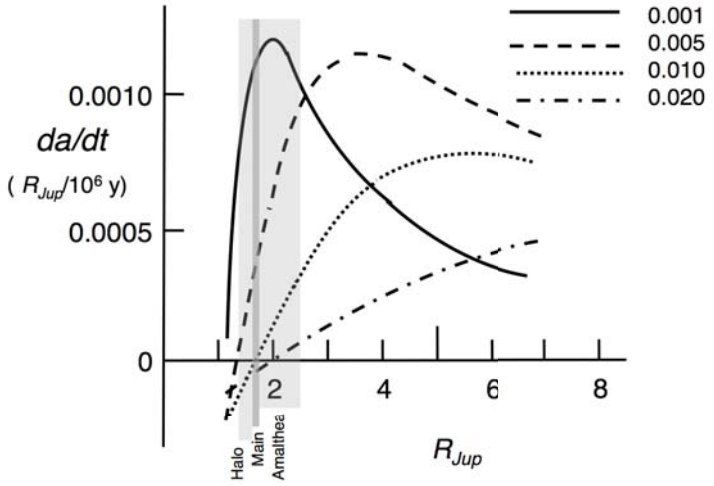

Fig. 7. Same as Fig. 3, but for Jupiter.

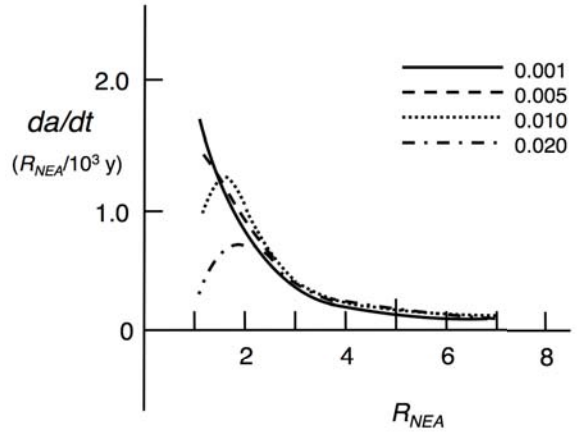

Fig. 8. Graph similar to Fig. 3, but for a hypothetical spherical NEA with radius 1000 m and density 2000 kg m^{-3} and in Earth's orbit with Earth's obliquity. The ordinate is in radii per 10^3 years, instead of per 10^6 years as in the other figures.

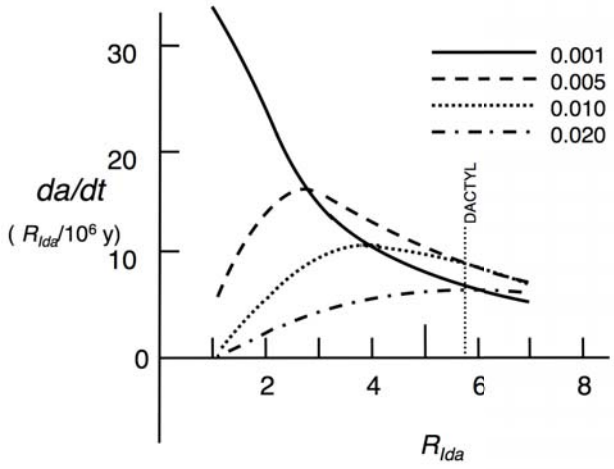

Fig. 9. Same as Fig. 3, but for asteroid 243 Ida, assuming Ida is a sphere.

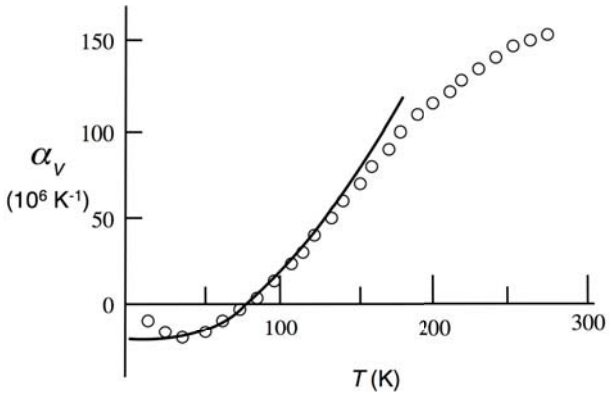

Fig. 10. The measured volume coefficient expansion for polycrystalline water ice as a function of temperature (circles) and the curve assumed here. The coefficient is negative for temperatures below 73 K, so that the thermal expansion effect would cause orbital decay rather than expansion for temperatures below this value.

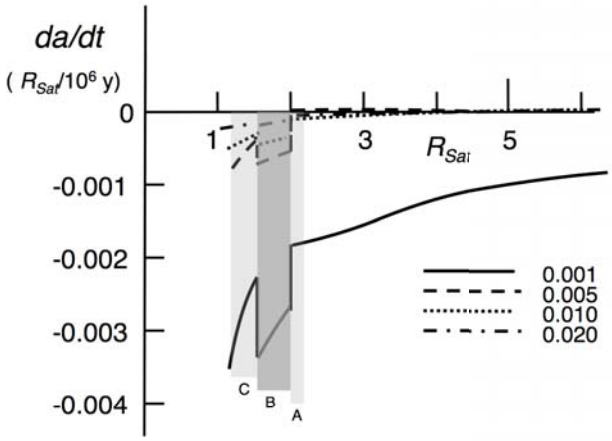

Fig. 11. Same as Fig. 3, but for ice particles orbiting around Saturn.

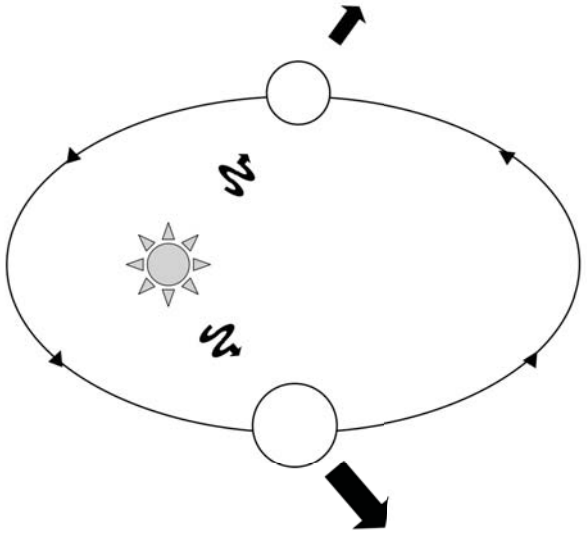

Fig. 12 Schematic of the thermal expansion effect for a meteoroid in an eccentric orbit about the Sun. The size of the arrows indicates the magnitude of solar radiation pressure on the meteoroid. As it approaches the Sun, sunlight (wavy arrows) heats up the meteoroid more and more, making it expand, increasing its cross-section and thus the force. The meteoroid achieves maximum size after perihelion passage, thanks to thermal inertia. Far from the Sun the weakened sunlight causes the meteoroid to contract, decreasing radiation pressure. The forces do not balance around the orbit, causing the orbit to expand secularly. The thermal expansion effect will also secularly change the orbital eccentricity.